Model synthetic pastes for low pH cements

E. Kangni-Foli, Stéphane Poyet, P. Le Bescop, T. Charpentier, F. Bernachy-Barbe, A. Dauzères, E. L'Hôpital, M. Neji, J.-B. d'Espinose de Lacaillerie

Model synthetic pastes for low pH cements

Kangni-Foli E. [1,2], Poyet S. [3], Le Bescop P. [3], Charpentier T. [4], Bernachy-Barbé F. [3], Dauzères A. [1], L'Hôpital E. [1], Neji M. [1], d'Espinose de Lacaillerie J.-B. [2]

(1) IRSN, Institute of Radiation Protection and Nuclear Safety, PSE-ENV/SEDRE/ LETIS, BP 17, F-92262 Fontenay Aux Roses, France

(2) Soft Matter Science and Engineering, UMR CNRS 7615, ESPCI Paris, Université PSL, 10 rue Vauquelin, 75005 Paris, France

(3) Des-Service d'Etude du Comportement des Radionucléides (SECR), CEA, Université de Paris-Saclay, F-91191, France

(4) NIMBE, CEA, CNRS, Université Paris-Saclay, CEA Saclay, F-91191 Gif-sur-Yvette Cedex, France

Corresponding author: Stéphane POYET

- Postal address: CEA Saclay, DES/ISAS/DPC/SECR/LECBA, B158 PC25, F-91191 Gif-sur-Yvette cedex, France.
- Email: stephane.poyet@cea.fr

Conflict of interest: none

Abstract

Model synthetic pastes were designed to obtain a simplified silica system that could be used in durability studies on materials with low calcium-to-silica ratios. The synthetic pastes made use of the well-known pozzolanic reaction between tricalcium silicate (C_3S) and nanosilica, covering calcium-to-silica ratios (C/S) from 0.8 to 3.0. The pure C_3S paste (C/S = 3.0) contained C-S-H and portlandite, while pastes with C/S $<$ 1.4 only included C-S-H. The pore solution pH directly correlated with the C/S ratio. The synthetic pastes demonstrated a mineralogy, a C-S-H structure, a mean chain length and pore network features that were similar to ordinary Portland cement (OPC) and low-pH materials, depending on their C/S ratios. The main shortcomings were: (1) high water-to-binder ratio and high superplasticizer dosage to maintain the workability of the synthetic pastes of low C/S ratios and (2) significant cracking of the pastes of low C/S ratios.

Keywords: Calcium-Silicate-Hydrate (C-S-H) – Model pastes – Microstructure – Mineralogy

1. Introduction

Despite its crucial societal importance, the chemical durability of concrete structures is difficult to predict. This is largely due to the conjunction of a metastable phase assembly in the binder with a multiscale mechanical and porous structure. Correctly predicting crack propagation or reactive transport for example, needs a thorough understanding of the governing phenomena across

several length scales [1]: the cement paste at the nano and meso scale [2], the aggregate and the interfacial transition zone at the meso scale [3,4], and finally the structure itself at the macroscale [5]. An unavoidable prelude to multiscale numerical modelling, thermodynamical or mechanical, is thus the understanding of the material at each scale taken separately.

Along this line, a lot of progress has been obtained in the last decades by focusing on concrete at the smallest scale: the mineralogical assembly of the cement paste [6–11]. An Ordinary Portland Cement (OPC) paste is in itself a highly complex heterogeneous system made of empty pores, water saturated pores, calcium silicate and aluminate oxides and carbonates. This has led researchers to further simplify the system by restricting the chemistry to the hydration products of tricalcium- (C_3S) or dicalcium- (β-C_2S) silicates [12–19]. It was thus possible to deconvolute the impact of silicates and aluminates chemistry and successfully rationalize non trivial behaviour such as induction and creep [2,19]. However, new needs in term of reduction of CO_2 emission or radioactive waste management has led to the development of low calcium and low pH cement formulation and in particular of the so-called low-alkalinity cements (LAC). Just as for OPC, the long-term prediction of the durability of low-pH cements requires the design of a model chemical system reproducing their main characteristics in terms of mineralogy and porosity.

For OPC, the paste formed by hydration of C_3S or β-C_2S constitutes a relevant model of the calcium silicate sub-system since it leads to the precipitation of the two main calcium-bearing hydrates of Portland cements, namely calcium-silicate hydrate (C-S-H) and portlandite (calcium hydroxide, CH). While C-S-H is largely responsible for the mechanical properties of the pastes, portlandite is a key component as it buffers the pH value at 12.5 (at 25°C). This latter fact is not true however for LACs which have very different specificities when compared to OPCs, the main one being the absence of portlandite and a pH of the pore solution (around 11) that is 1 to 3 points lower than in usual cements (≈13.5) [20–24]. Such low pH values are commonly achieved by adding significant amounts of secondary cementing materials poor in calcium [25]. As a result, the C/S ratio of the paste is much lower than usual and the development of another chemical model is needed. This is particularly important since the long term durability of LAC is still an open question, especially with respect to carbonation which is highly pH dependent. Consequently, the aim of this paper is to synthesize and describe model synthetic low-pH porous systems representative of LAC pastes.

Several attempts have already been presented in the literature. Firstly, Chen *et al.* [26,27] exposed C_3S hardened pastes to ammonium nitrate (6M) in order to dissolve portlandite and lower the CaO/SiO_2 ratio of the C-S-H. Alternatively, other authors created porous compacts of C-S-H powders obtained by aqueous mineral synthesis in excess water [28–37]. Each of these methods demonstrated a main drawback inherent to their fabrication methods, *i.e.* the chemical attack or the mechanical compaction may induce a dissimilarity in the porous medium with regard to that generated by hydration. The chemical attack alters both the hydrates [38] and the pore network [39]. For compacts, comparison with hardened cement pastes does not provide strong evidence of their full representativeness [40]. In addition, compact disintegration subsequent to water immersion has already been observed, which makes them unsuitable for transport modelling [30].

More recently, it was shown that pastes made of C-S-H with different C/S ratios could be obtained using a combination of calcium oxide or hydroxide and amorphous silica mixed with water [41,42]. Due to the high water demand of the silica powder [43], the water to solid ratios were high (from 1.1 to 2.0) but could be reduced using a superplasticizer [41]. Chemical analysis of paste obtained in that manner revealed scattered C/S ratios. For instance, in [41], the paste with an average C/S ratio of 1.25 includes areas with C/S ratios of 0.80 and others with C/S of 1.50. This could be the expression of a limited control of the pastes' local chemistry as hydration is known to be controlled by the dissolution rate of C_3S [44–46] which indirectly affects the

development of hydrate microstructures [47–49]. The scatter itself is not an issue because it is representative of real materials [50]. However, within the scope of laboratory studies, more narrowly distributed C/S ratios could be preferable as they might simplify interpretation of the results (for example to study the influence of the C/S ratio on the carbonation rate or the mechanical properties of C-S-H).

In this study, we kept the smart idea of Kunther et al. [41] and Maddalena et al. [42] for obtaining pastes by exploiting the pozzolanic reaction of silica but we investigated another route by replacing $CaO/Ca(OH)_2$ by tricalcium silicate. We then synthesized a series of model pastes of controlled chemistry with narrowly distributed C/S ratios of averages between 0.8 and 3.0. The methodology used to prepare the model pastes is described and their main chemical, mineralogical and microstructural properties are detailed. Finally, the relevance of the pastes as model subsystems for real LAC pastes is discussed.

2. Materials and methods

Synthesis of the model synthetic pastes

The pastes were prepared using stoichiometric amounts of finely ground C_3S and amorphous nanosilica (SiO_2) in order to maximise the hydration rate [51–53] and ensure complete silica reaction [22]. Triclinic C_3S was provided by Mineral Research Processing (Meyzieu, France) and presented a specific area of 4600 cm^2/g. The nanosilica was Rheomac AS 150, provided by BASF in the form of an aqueous suspension (50 wt%) with a median diameter D50 equal to 100 nm. The workability of the fresh mix was adjusted using a commercial polycarboxylate superplasticiser (MasterGlenium Sky 537 from BASF). The pastes were prepared in batches of 1.40 L using a planetary mixer. Before using expensive C_3S, tests were conducted using OPC with a similar specific surface to that of C_3S. The tests aimed at determining the most appropriate batching sequence, water-to-binder ratio (w/b) and superplasticiser dosage. There was no common workability objective for all the pastes. Our main goal was to obtain pourable pastes: this was easy without nanosilica but proved to become more and more difficult as the C/S ratio was decreased. The resulting compositions were then tested using C_3S and modified accordingly. The pastes incorporated significant amounts of nanosilica (up to 42 wt% for C/S = 0.80, see Table 1); this induced two major issues: (1) the high water demand of nanosilica [54,55], and (2) the significant flocculation of nanosilica in the presence of calcium ions [56,57]. Consequently, the w/b ratio and the SP dosage had to be increased when the C/S decreased. In the case of the paste with a C/S ratio of 0.80, the w/b ratio and SP dosage reached high values, i.e. 0.78 and 8.0% respectively. Table 1 gives the formulation of the pastes that we were able to produce. The exact batching sequence is provided in the Supplementary material section.

Table 1: Composition of the model pastes for 1L

C/S ratio	**3.00**	**1.40**	**0.95**	**0.87**	**0.80**
C_3S (g)	1218.8	791.7	586.0	563.9	506.2
Colloidal silica slurry (g)	0.0	475.8	664.5	726.3	734.3
Added water (g)	609.4	379.9	264.1	239.3	244.5
w/b ratio	0.50	0.63	0.73	0.72	0.78
Superplasticiser (wt% of binder)	0.0	3.0	8.0	7.0	8.0
Batching time (min)	5	8	15	17	20

Reference cement pastes

To assess the representativity of the synthetic pastes, two cement pastes based on CEM I were prepared: an OPC paste (CEM I) and a reference LAC, namely the T_1 blend (mix of CEM I, silica fume and fly ash, see Table 2) proposed by Codina *et al*. [20] and studied later [6,23,58,59]. The reader is referred to the Supplementary materials section for more detail about elemental composition.

Table 2: Composition of the reference pastes for 1L

Reference materials	**T_1 (CEM I + SF + FA)**	**CEM I**
C/S ratio	0.53	3.3
Cement (g)	470.4	1396.7
Fly ash (g)	378.2	-
Silica fume (g)	406.8	-
Added water (g)	502.2	558.0
w/b ratio	0.40	0.40
Superplasticiser (wt. % of binder)	1.0	0.0
Batching time (min)	5	5

The SP dosage of the model synthetic pastes - especially for the lower C/S ratios (0.95, 0.87 and 0.80) - was quite high compared to the reference cement pastes. It should be pointed out that nanosilica was incorporated in the model paste, whereas silica fume and fly ash were used in the reference paste. This is why the SP dosage had to be increased to partially offset the water demand of the fine nanosilica particles.

Mineralogical and chemical characterisation

The pH of the pore solution was measured using the *ex situ* leaching (ESL) method [60–62]. Owing to the absence of alkalis in the binders, ESL is known to yield similar results with respect to the reference method (extraction).

Thermogravimetric analysis (TGA) was performed using a Netzsch STA 409 PC Luxx apparatus. Analyses were run under a constant N_2 flowrate (80 ml/min). The weight losses were recorded from 25°C to 1150°C with a heating rate of 10°C/min [63]. The quantification of portlandite (using the tangential method [64]), expressed in mol/L of paste is obtained by considering the weight loss (between 420-580°C) associated to 120 mg of powdered sample of each model paste and their saturated volumes and apparent densities.

Powder X-ray diffraction (XRD) patterns were collected using a XPD PANalytical X'Pert diffractometer with a Bragg-Brentano geometry in an Θ-Θ configuration and a Cu K_α radiation source (45 kV, 40 mA).

Silicon magic-angle spinning nuclear magnetic resonance (^{29}Si MAS NMR) single-pulse data was collected using a Bruker Avance III 500 spectrometer operating at the Larmor frequency resonance of 99.3 MHz. Conditions were set to π/2 pulses of 3.5 μs, recycle delays of 20 s, spinning in 7 mm zirconia rotor at 5.5 kHz, and a minimum of 4000 scans for each spectrum. Tetramethylsilane was used as an external standard (0 ppm) to report the chemical shifts. The ^{29}Si MAS NMR results were processed using an internally developed software [65,66]. The spectra

were fitted using gaussian-lorentzian lineshapes with chemical shifts and widths kept identical for all pastes (see Table 4 and Table S 1).

A ZEISS EVO MA15 scanning electron microscope (SEM) equipped with a Quantax detector for energy-dispersive spectrometry (EDS) was used for chemical mapping together with backscattered electrons (BSE) imaging. Acquisitions were collected at 15 kV and 1 nA. Pastes were freeze-dried, mounted using epoxy resin, and then polished using an alcohol-based diamond suspension. Grids of 609 points recorded at 200× magnification were acquired for each sample. Due to the working voltage used, an electron–matter interaction depth of about 1-10 µm within the material was generated.

Microstructure characterisation

Microtomographic projections were acquired on a Bruker SkyScan1173 device equipped with a flat detector (2240 × 2240 pixel) using the following operating conditions: 115-130 kV and 61-69 µA. We obtained 360° scans with a rotational step of 0.3°, exposure time of 1100 ms, a frame averaging from 8 to 10, and images with a pixel size of 16.8 µm.

The porosity and density of the pastes were obtained using the buoyancy method. Firstly, cylinders were re-saturated under vacuum and water [67], and their volume and weight were measured. They were then dried at 80°C in the presence of $CaCl_2$ and 105°C until constant weight was reached in order to compute porosity. The rationale behind the choice of these temperatures is that at 80°C, the hydrates are fully preserved but some water remains in the porosity, while at 105°C, all water is removed but the hydrates are partially dehydroxylated.

The pore entry size distribution (PSD) of the pastes was characterised using mercury intrusion porosimetry (MIP) with a Micromeritics Autopore IV. Prior to the tests, the specimens were crushed into centimetric pieces that were immersed in liquid nitrogen and then freeze-dried for 24 hours.

The C-S-H content of the pastes was estimated using the method proposed by Olson and Jennings [68] based on the quantification of the water content at 20% RH. Here we did not strictly follow the protocol recommended by Olson and Jennings. Rather we estimated the water content at 20% RH using a desorption experiment and a sorption balance (DVS Advantage). Acquisitions were run at 25°C ±0.1°C, and the automatic 'dm/dt' mode was set for the relative humidity (RH) decrease. Prior to analysis the pastes were crushed and sieved in a CO_2-free glove box. Particles exceeding 150 µm were eliminated by sieving and the powders saturated using deionized water. More details can be found in [69]. Such an approach offered a very significant gain of time but might have overestimated the C-S-H content due to the hysteresis between the adsorption and desorption path. The reader should also be aware that the method of Olson and Jennings assumes that the C/S ratio of the C-S-H is equal to 1.7. It is thus well suited for the C_3S and CEM I pastes but subject to caution for other formulations. This might have induced additional uncertainties in the C-S-H quantification process. This point would require more attention but is not addressed in the present work.

3. Results

Reference cement pastes

The characteristics of reference cement pastes, OPC or LAC were fully in line with what was expected from the literature and need not to be extensively reported here (see later the NMR spectra in Figure 3, the MIP in Figure 8 and XRD in Figure S 2). The main difference in terms of mineralogy for the LAC compared to OPC is the absence of portlandite and the presence of calcium-bearing amorphous silica (silica gel) and remnants of amorphous silica phase such as fly ash and silica fume that have not reacted with calcium. Furthermore, the low C/S ratio resulted in longer dreierketten chains in the C-S-H of the LAC cement paste. The porosity of the LAC paste presented a more refined pore structures due to pore filling by precipitation of pozzolanic C-S-H.

Mineralogy of the model synthetic pastes

X-ray diffractograms of the model pastes with C/S ratios from 0.80 to 3.00 are shown in Figure 1. The paste with a C/S ratio of 3.00 corresponds to the sample prepared without silica. Logically, its diffractogram corresponded to what was expected from the hydration of pure C_3S, *i.e.* it mainly showed diffraction peaks of the portlandite and C-S-H patterns [70–73]. Only traces of reflections corresponding to remaining C_3S were detected, indicating that hydration was almost complete [18]. Pastes with C/S ratios of 1.40 mainly displayed C-S-H signals and traces of portlandite and unreacted C_3S. Finally, for C/S ratios lower than 1.40, the diffractograms only exhibited the C-S-H diffraction pattern.

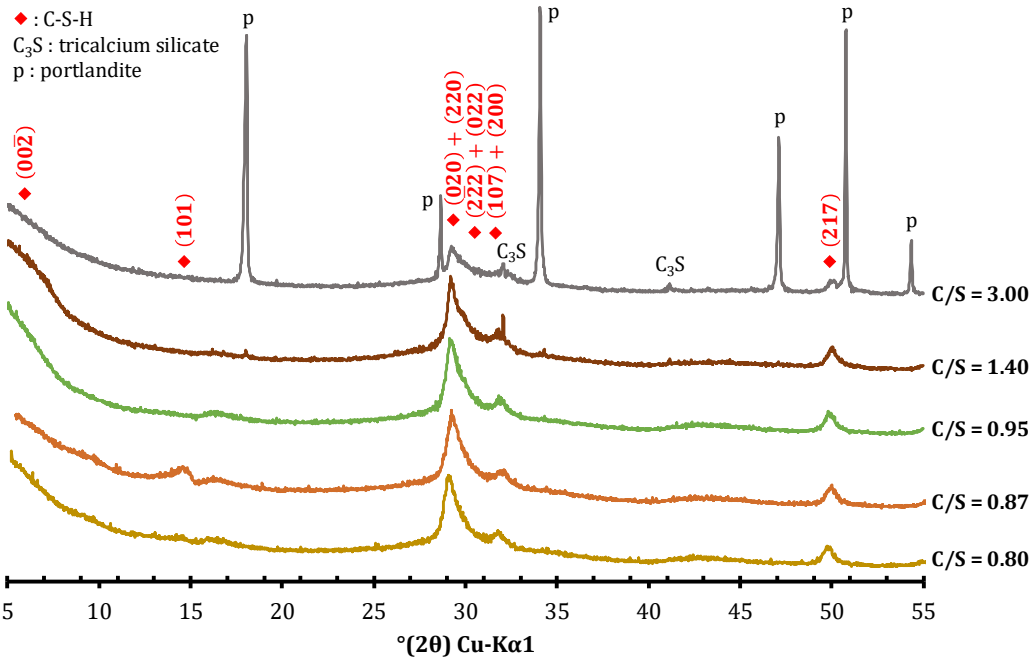

Figure 1: XRD patterns of the synthetic pastes. As the C/S ratio decreases, Portlandite reflections progressively disappeared from the diffractogram. While still barely visible at C/S 1.4, they were absent for synthetic pastes of lower C/S ratios. C-S-H indexing was based on [74–76]*, ICDD files CH: 44-1481, C_3S: 31-0301.*

TGA confirmed the results obtained using XRD. The portlandite content measured in the C_3S paste (7.3 mol/L of paste, cf. Table 3) was very close to that of a fully hydrated C_3S paste (7.0 mol/L of paste with C-S-H with C/S = 1.70). For C/S ratios of 1.40, losses associated with C-S-H and traces of portlandite were observed (Figure 2). For C/S ratios lower than 1.40, the

thermograms only exhibited signals related to C-S-H (see the C/S = 0.80 thermogram in Figure 2).

Table 3: Composition and properties of the synthetic and reference pastes obtained by TGA, µCT and the buoyancy method. The C-S-H content was obtained following the method of Olson and Jennings [53]. (see Materials and method section)

	Model pastes					Reference pastes	
C/S ratio	**3.00**	**1.40**	**0.95**	**0.87**	**0.80**	**CEM I**	**T_1**
C/S of the C-S-H	1.70	1.40	0.95-1.10	0.87-1.00	0.80-1.00	1.70	[0.8-1.1]*
Porosity (80°C)	38%	52%	57%	57%	58%	36%#◦	41%#◦
Porosity (105°C)	41%	56%	61%	61%	62%	38%#◦	43%#-46%⁂
Saturated density	1.89	1.76	1.68	1.67	1.63	2.04⁂-2.05#	1.73⁂-1.77#
C-S-H (mol/L of paste)	5.6	7.0	6.7	7.0	6.3	5.1⁂-5.2◦	7.4⁂-7.6◦
CH (mol/L of paste)	7.3	0.0	0.0	0.0	0.0	5.6⁂-5.3#	0.0*#
Cracking (µCT)	-	-	+	++	++	-	-

- no crack observed + few small cracks ++ several extended cracks

data from *[77], ◦[23], *[20], #[78] ⁂[79]

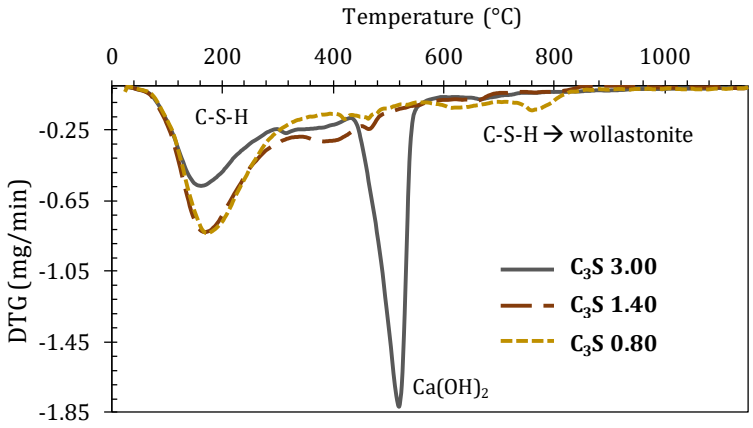

Figure 2: DTG of the model pastes. Besides losses due the removal of water within C-S-H, the typical thermal loss of portlandite was massively observed in the C_3S paste. In contrast, only a residual portlandite content was evidenced in the C/S = 1.40 paste, and it totally disappeared at lower C/S ratios.

The ^{29}Si MAS-NMR spectra of the pastes are shown in Figure 3. The spectra of the higher C/S ratios (3.00 and 1.40) samples exhibited the usual resonances attributed to silica tetrahedra sharing one (Q^1) or two (Q^2) oxygen atoms with another tetrahedra at -79.19 ppm and between -83 and -86 ppm respectively [41,80,81]. As expected, the decrease in the C/S ratio resulted in a relative increase in the Q^2 contribution reflecting the increase of the length of the dreierketten chains of the C-S-H. The spectra of pastes with C/S ratios lower than 1.40 predominantly showed Q^2 silicate tetrahedra. In that case, the bridging and the paired tetrahedra of the dreierketten chains of C-S-H (Q^{2b}, Q^{2p}) could also be distinguished. According to the literature, they occur around -83.0 ppm and -85.0 ppm [82,83]. A broad contribution in the frequency range of Q^3 tetrahedra (-90 to -100 ppm) was detected in samples with C/S below 0.95 in increasing amounts as the C/S ratio decreased (and the silica content of the formulation increased). Q^3 coordination has been proposed in C-S-H of low C/S ratios but are expected to be a minor occurrence in the absence of aluminium [84]. Without further evidence, and considering its breadth, it was thus preferred to attribute tentatively this resonance to the occurrence of an amorphous silica (Q^3gel). The

distribution of the silicate tetrahedra environment as a function of the C/S ratio was obtained by decomposition of the ^{29}Si resonances and reported in Table 4. Examples of the decomposition procedure and results are provided as Supplementary materials.

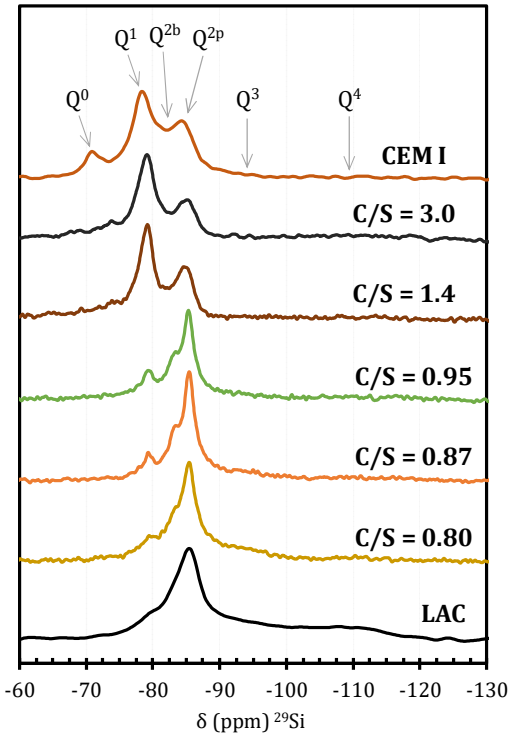

Figure 3: ^{29}Si MAS-NMR spectra of the series of model synthetic pastes with varying C/S ratios and of the reference pastes. Synthetic pastes of higher C/S ratio had lower proportion of Q^2 (middle chain) to Q^1 (end chain) silicate coordination evidencing the expected decrease in dreierketten chain length with increasing C/S ratios. The spectra of the end members of the synthetic series where very similar to the ones of the reference pastes. The reference CEM I and LAC pastes showed Q^0 on the one hand, and Q^3 and Q^4 resonances on the other hand, due to unreacted calcium silicates and to unreacted silica fume and fly ash respectively.

Table 4: Relative occurrence of silicate environments in the reference and model pastes from ^{29}Si MAS-NMR. For the LAC paste, unreacted fly ash was observed in the LAC paste characterized by Q^3 and Q^4 broad peaks overlapping with almost all other resonances.

Paste		**Q^0**	**Q^1**	**Q^{2b}**	**Q^{2p}**	**Q^3 (*)**	**Q^3 (FA)**	**Q^4 (FA)**	**Q^4 (SF)**
δ (ppm)		-71.6	-79.2	-83.1	-85.4	-92.0	-90	-104	-110.0
Model pastes	0.80	-	10%	21%	43%	26%	-	-	-
	0.87	-	14%	25%	50%	11%	-	-	-
	0.95	-	16%	25%	51%	8%	-	-	-
	1.40	-	52%	13%	29%	6%	-	-	-
	3.00	-	68%	11%	21%	-	-	-	-
Reference pastes	CEM I	11%	56%	11%	22%	-	-	-	-
	LAC	-	8%	17%	34%	6%	15%	15%	5%

* in the presence of Q^3gel it was not possible to determine the contribution of the Q^3 environments: the Q^3 column then includes the contributions of Q^3 and Q^3gel (when present, i.e. for C/S ≤ 0.95)

Figure 4 shows the chemical analysis (SEM) results obtained for the model synthetic paste with the lowest (0.80) C/S ratio. A typical electron density contrast image given by BSE mapping is shown in Figure 4(a) and the subsequent mapping of the C/S ratio distribution obtained using

EDS on a 400×550 µm² (21×29 points) subzone is displayed in Figure 4 (b). These results revealed an almost homogeneous distribution of the C/S ratio at the scale of EDS sampling (20×20 µm² surface with an analysis depth of ~1-10 µm) with a limited standard deviation (coefficient of variation CV = 5%).

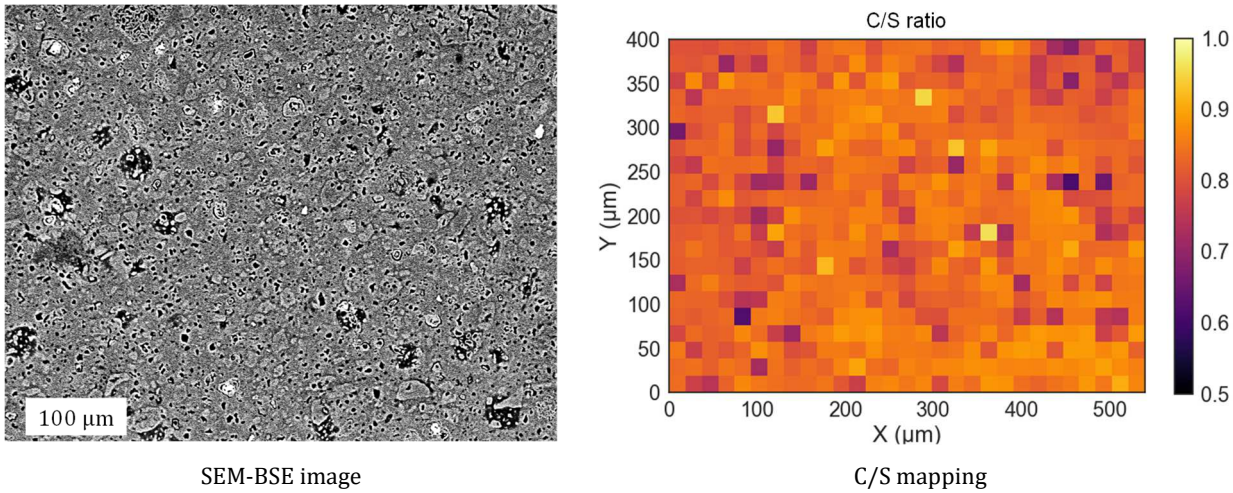

SEM-BSE image C/S mapping

Figure 4: SEM examination of the synthetic paste with a C/S ratio of 0.80. At the scale of the EDS mapping, the paste appeared very homogeneous in composition.

Figure 5 and Figure 6 show the C/S ratio occurrence in each model synthetic pastes. All the samples presented average C/S ratios that were very close to targets except the C_3S paste results that were scattered over a wider range probably due to the expected precipitation of portlandite crystals. In contrast, the other samples were narrowly distributed with a CV between 5% and 6%, with the exception of the paste with a C/S ratio of 0.95 with a CV of 12% (Table 5).

Table 5: Mean value and standard deviation of the C/S ratio distribution of the model pastes

Target C/S	**0.80**	**0.87**	**0.95**	**1.40**	**3.00**
Average C/S value	0.83	0.89	1.06	1.36	2.53
Standard deviation	0.04	0.05	0.10	0.08	0.31
Coefficient of variation (CV)	5%	6%	9%	6%	12%

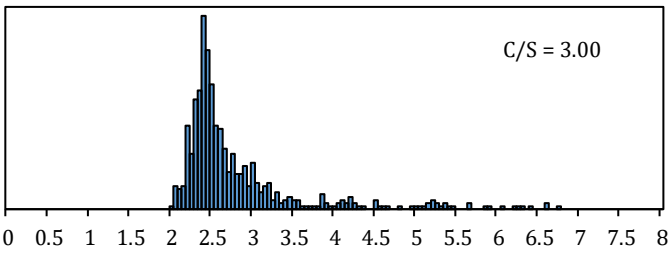

Figure 5: Distribution of the CaO/SiO_2 ratio obtained using SEM-EDS for the C_3S paste

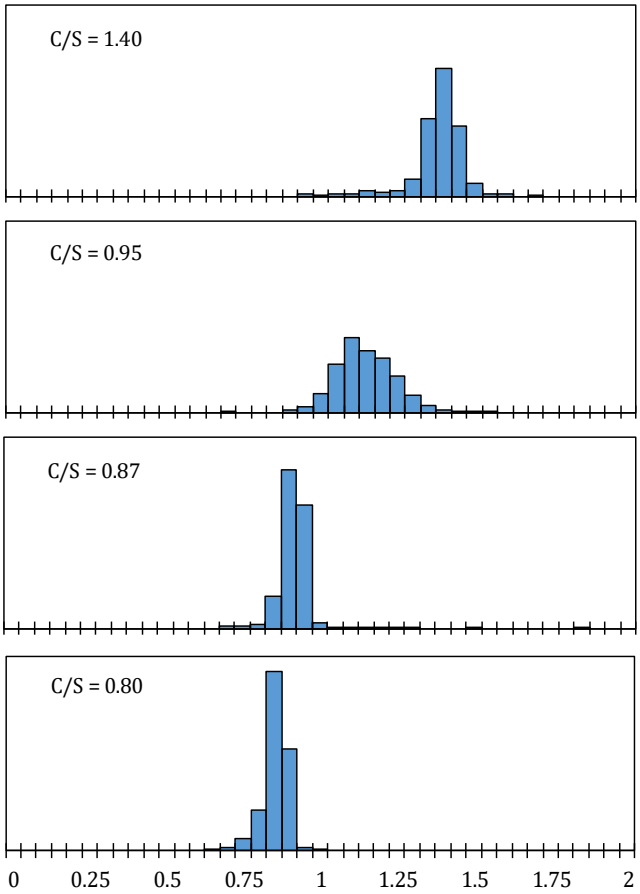

Figure 6: Distribution of the CaO/SiO_2 ratios obtained using SEM-EDS for the synthetic pastes for C/S ≤ 1.40

Representativity of the chemistry and mineralogy of the model synthetic pastes

XRD and TGA proved that the pastes with C/S ratios lower than 1.40 contained C-S-H only, whereas the paste based on pure C_3S showed the concomitant precipitation of portlandite. This is in line with what is expected from a LAC and a CEM I paste respectively. ^{29}Si MAS-NMR analysis of the pastes evidenced C-S-H silicates silicon environment distribution evolving continuously with the C/S ratio between what is observed in a LAC and in a CEM I paste. Furthermore, EDS chemical analysis highlighted the relative homogeneity of the C-S-H pastes with actually an even narrower scatter in the C/S ratios, compared to those usually observed in cementitious materials but in line with what is observed in pure calcium silicate hydrate pastes [85,86]. In that respect, the synthetic pastes formed a representative model of the silicates mineralogical assembly found in LAC pastes.

The pH values of the pore solutions obtained using the ESL method are given in Figure 7. For the purpose of comparison, the values are plotted together with literature data and with the model proposed by Haas & Nonat [87]. The pH of the synthetic pastes pore solution (measurement made at 20 ± 2°C, with temperature compensation) demonstrated a decrease while the target C/S ratios were lowered. Our data falls within the variance shown by literature data and confirmed that the model synthetic pastes also successfully reproduced the low-pH character of LAC pastes.

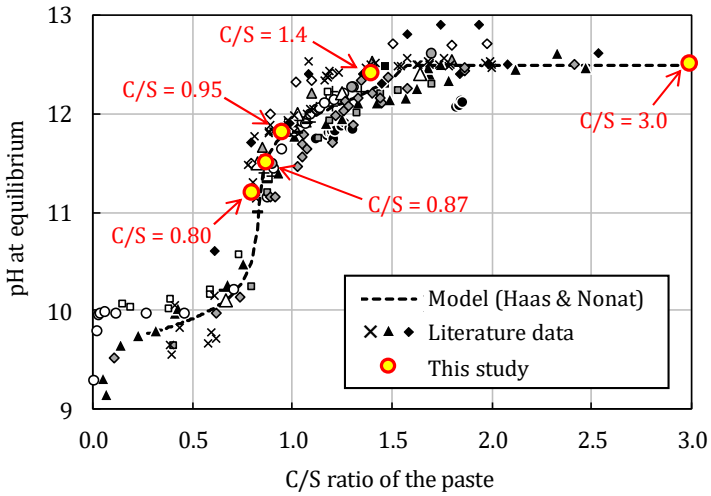

Figure 7: pH of the pore solutions of the synthetic pastes measured using the ex-situ leaching method, redrawn from [12,88–98] *along with the model proposed by Haas & Nonat [87]. The pH of the pore water of the synthetic pastes satisfactorily reproduced observations reported in the literature and conformed to the predictive model.*

Microstructure of the model synthetic pastes

The saturated density, porosity and chemical composition (C-S-H and CH contents) are reported in Table 3. The estimated C-S-H content was higher for the pastes with C/S ratios lower than 3.00: this was in line with the expected formation of extra C-S-H from silica through pozzolanic reactions. The paste porosity increased and the density decreased when the target C/S ratio decreased. However, as the C/S ratio was decreased by addition of nanosilica, a concomitant increase of the w/b ratio was needed to maintain the workability of the synthetic pastes. The variations in porosity and density was thus probably more associated to the water content than to a change of chemistry. Figure 8 illustrates the pore size distribution (PSD) of the synthetic pastes obtained by MIP. For sake of comparison, the cement pastes are also presented. While the PSD of the pastes with C/S ratios of 3.00 and 1.40 revealed the expected presence of the C-S-H gel porosity in the 10 nm range, the pore structure was considerably refined for the lower C/S ratio. Again, this could be related to the filling effect induced by the precipitation of pozzolanic C-S-H. The increase of the porous volume on the other hand was probably related to the increased w/b ratios of the synthetic pastes.

Representativeness of the microstructure of the model synthetic pastes

The synthetic pastes had a narrower PSD and a higher pore volume than the one of the reference LAC paste, again due to the w/b ratio needed for their mixing as previously stated in the Materials and methods section. However, the PSD of the low C/S synthetic pastes had no pores with critical entry diameter above 10 nm (Figure 8). This was reminiscent of what is observed in LAC pastes were the paste capillary porosity is considerably reduced by the pozzolanic reaction.

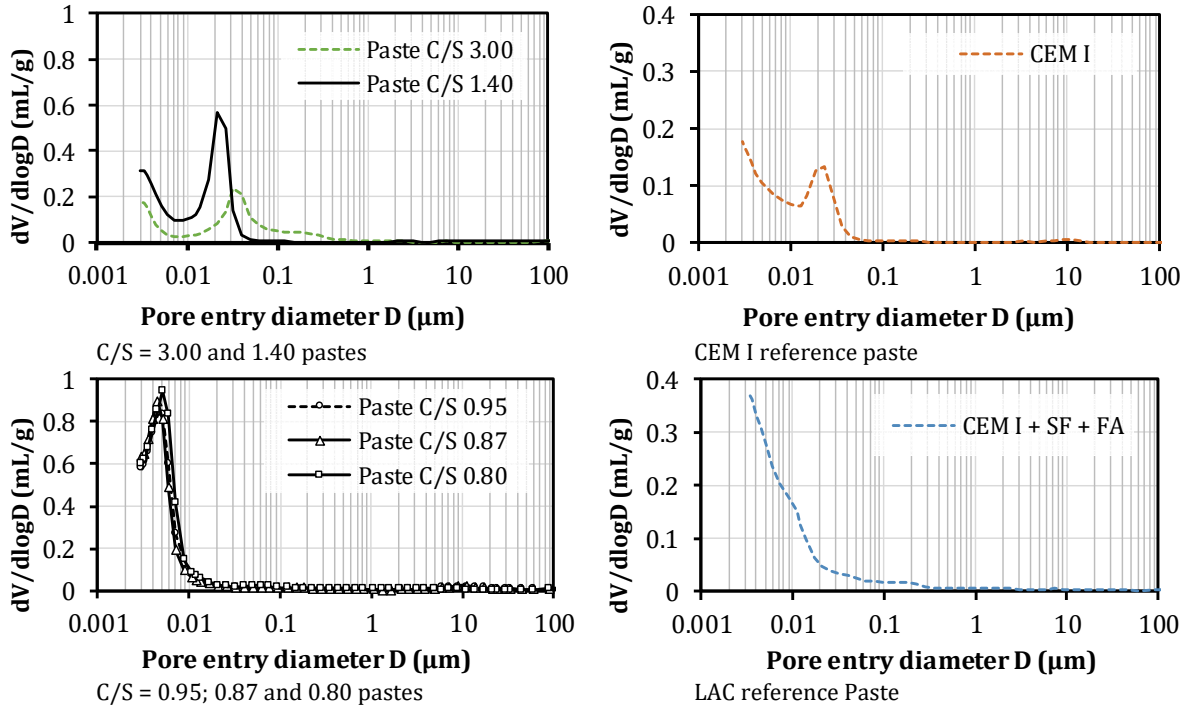

Figure 8: PSD from mercury intrusion porosimetry for reference (right) and synthetic pastes (left).The PSD of the high C/S ratio synthetic pastes conformed to the one of an OPC (CEM I) paste, and the one for the lower C/S ratios to the one of the LAC (CEMI+SF+FA) reference paste.

X-µCT scans of samples with C/S ratios of 1.40, 0.87 and 0.80 are shown in Figure 9. The C/S ratio of 1.40 showed a homogenous matrix, almost exempt of air bubbles. No cracks were observed in the pastes with the higher C/S ratios (3.00 and 1.40) (image a). The pastes with lower C/S ratios of 0.87 and 0.80 exhibited more contrasted features with darker spots observed in the matrix; these areas could be attributed to silica-enriched areas, thus supporting the NMR observation of a small amount of unreacted silica. These pastes also contained several bubbles due to reduced workability induced by the high amount of nanosilica in their formulations. Furthermore, they had an extended crack network (images b, c). The cracks made the samples very brittle and it was necessary to be extremely careful when handling the low C/S synthetic pastes and they proved to be very difficult (almost impossible) to cut without breaking. This was believed to be due to the polymerisation of the silica chains of the C-S-H induced by the incorporation of silica in the C-S-H, which is known to generate significant volume changes [27] and might result in densification and internal stress during maturation of the lower C/S pastes. It must be mentioned though that the unusually high superplasticizer dosage might have played a role in the brittleness of the pastes of low C/S ratios even though the literature remains scant about this subject. Ramachandran [99] showed that lignosulfonates had strong and irreversible interactions with the C-S-H but it was later proven that more recent compounds [100] such as melamine sulfonates and polyethylene oxide phosphonates did not affect the C-S-H [101,102]. The results are however not so clear with polycarboxylic ethers [103–106]. This point would require more attention in the future.

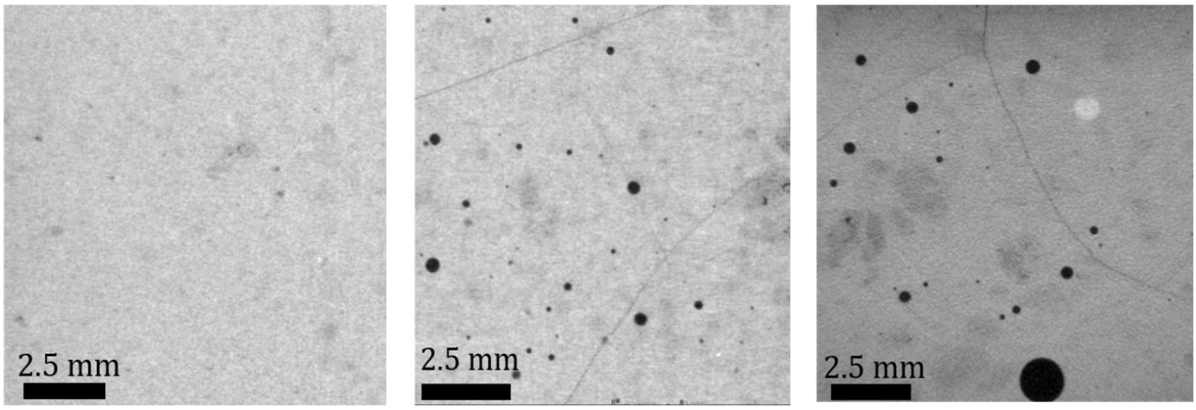

(a) C/S = 1.4 (b) C/S = 0.87 (c) C/S = 0.80

Figure 9: X-ray µCT scans images of 3 samples of the synthetic pastes series. Significant cracking was observed in paste with lower C/S ratios

4. Discussion

At first sight and as exposed in the results section, the mineralogical assembly of the model synthetic pastes seemed to correctly represent the one expected from LAC pastes. To examine further this issue, the atomic and molecular structure of their C-S-H, as revealed by NMR, was examined in details and compared to the ones of cement pastes.

It is common practice to estimate the mean chain length (MCL) of the C-S-H dreierketten silicate chains from the distribution of the silicate environment obtained by ^{29}Si MAS-NMR. Accordingly, the MCL was obtained in the synthetic pastes using the C-S-H crystal chemical model of Richardson [107]. Indeed, the following simplified expression (Equation 1) relates the MCL to the NMR relative intensities of the Q^1 and Q^2 (Q^{2b} and Q^{2p}) environments:

$$MCL = 2\left(\frac{Q^1+Q^{2b}+Q^{2p}}{Q^1}\right) \qquad \textit{Equation 1}$$

Figure 10 shows the C-S-H MCL of the pastes depending on their targeted C/S, along with predictions from the Richardson tobermoritic model and some data from literature. In the higher C/S range (above 1.5), the C-S-H of the pastes demonstrated a chain length variation that was not fully described by the simple tobermoritic model. This behaviour is similar to what is commonly observed in cement paste and is rationalized through an additional charge compensation mechanism, which involved calcium insertion in interlayers [107,108]. However, within the lower C/S domain (C/S ≤ 1.0), the mean chain length of the C-S-H in the synthetic pastes followed reasonably well the prediction of a tobermoritic behaviour.

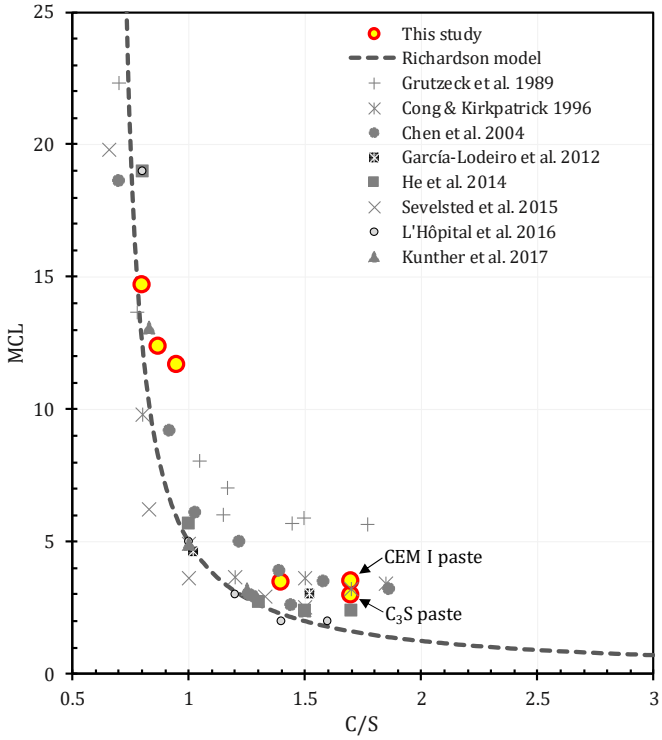

Figure 10: C-S-H mean chain length of the synthetic pastes (from ^{29}Si MAS NMR) along with literature data [12,41,83,89,90,107,109–111]. The MCL obtained for our model pastes correlated well with the MCL of the cementitious materials reported in the literature

In the crystal-chemical structure provided by Richardson [107], the C-S-H gel is considered as a structurally defective form of tobermorite. The structural model describes the C-S-H structure (MCL, C/S ratio) based on the rate of occupancy of the vacant sites. Adopting this structural model, one can in principle back-calculate the C/S ratio of the C-S-H from the NMR spectrum. Practically speaking, following Richardson [107], the C/S ratio (Equation 2) and the mean chain length (MCL) were calculated using:

$$\mathrm{MCL} = \frac{1-\nu}{\nu} \quad \text{and} \quad \frac{\mathrm{C}}{\mathrm{S}} = \frac{\frac{2}{3}+\nu}{1-\nu} \qquad \textit{Equation 2}$$

where the fraction of vacant sites ν (Equation 3) within the C-S-H structure was evaluated by decomposition of the NMR contributions:

$$\nu = \frac{\frac{1}{2}\mathrm{Q}^1}{\frac{3}{2}\mathrm{Q}^1+\mathrm{Q}^2+\mathrm{Q}^3} \qquad \textit{Equation 3}$$

Excluding the Q^3 resonance attributed to a silica gel, the C/S ratio predicted from the Richardson defective tobermoritic model agreed reasonably well with the bulk C/S ratio of the pastes (Figure 11). This meant not only that the pastes were indeed devoid of portlandite, as seen by XRD and TGA, but also that their C-S-Hs' structure behaved identically to the ones encountered in real (LAC) cement paste where the defective tobermorite structural model is now well established [112]. This confirmed the representativeness of the mineralogy of synthetic pastes' silicate with respect to the one of LAC paste of identical C/S.

Finally, it might be useful to stress the fundamental difference between the C/S pertaining to NMR on the one hand and to SEM-EDS analyses and to the pH of the pore solutions on the other hand

(Figure 11). NMR analyses account for properties at the molecular scale and thus reflects the local availability of Ca and Si at the C-S-H scale. In contrast pH is a macroscopic property reflecting phase equilibria within the sample, namely C-S-H and portlandite. Lastly, SEM-EDS probes the sample at the micro scale and its mean value is thus expected to reproduce the bulk composition of the paste within experimental errors. These considerations are illustrated in Figure 11 where C/S ratios obtained by SEM-EDS and by modelling the ^{29}Si NMR spectra as well as the pH are compared to the bulk C/S ratio recalculated excluding the silicon incorporated in amorphous silica (estimated from the ^{29}Si NMR spectra). The latter C/S ratio was taken as being the one of the C-S-H / portlandite assemblage.

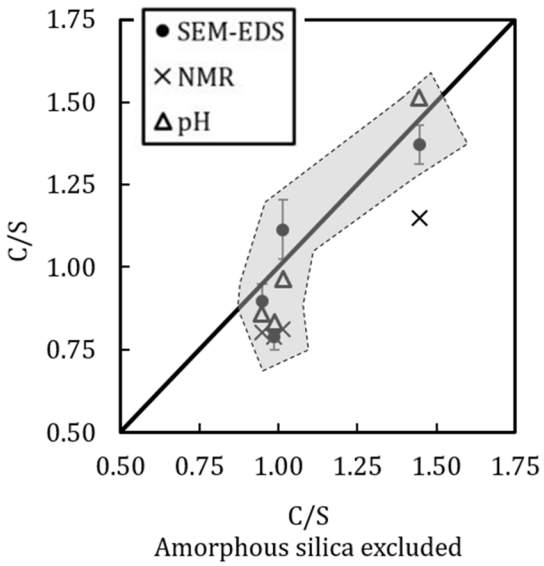

Figure 11: Comparison of the bulk C/S ratios (excluding the silicon in the amorphous non C-S-H part of the sample, unreacted products or silica gels, estimated by ^{29}Si NMR) with the results of SEM-EDS and with the ones expected from modelling pH measurements (Haas and Nonat model) and NMR ones (Richardson model). Error bars on the SEM-EDS data correspond to the measured coefficient of variation (see Table 5). The accuracy of the pH measurements are +/- 0.05. This translates into an error of about +/- 0.01 in the C/S values given by the Haas and Nonat model (Figure 7). The NMR intensities are obtained with an accuracy of about 10% leading to an error of about +/- 0.05 in the C/S values given by the Richardson model (Figure 10).

5. Conclusions and perspectives

In this study we prepared a series of synthetic pastes with C/S ratios between 0.8 and 3.0 and evaluated its potential as a model silicate subsystem for LAC pastes. From a chemical and mineralogical standpoint, the synthetic pastes appeared as good models, reproducing satisfactorily the mineralogical assemblage. The structure of the C-S-H and the amount of portlandite formed, or not, followed what was expected from a LAC paste. Furthermore, the pH of the pore solutions also conformed very well to predictions with respect to the C/S ratios. This objective was met by choosing C_3S and nanosilica with the appropriate dosage. However, the use of nanosilica induced a high water demand and the formulation had to be optimized through an increased w/b ratio and high superplasticiser dosage. Consequently, the synthetic pastes had a higher pore volume. All the while, the evolution of the PSDs of the synthetic pastes with the C/S ratio was similar to those of the reference pastes. The protocol proposed in the present work thus constituted an interesting route to design synthetic pastes to model the silica subsystem of LAC

pastes. This might be particularly useful to model experimentally complex reactive transport within low-pH cements, such as carbonation. In addition, since a narrow variation of C/S ratios was obtained for each targeted value, this series could be suitable for studying the influence of the C/S ratio on various properties of cementitious materials, such as the C-S-H gel mechanical properties. Such studies will have to factor in however, the fact that the pore volume of the model pastes were much higher than those usually encountered in real cement pastes.

The present work intended to study specifically the role of the C/S ratio of the silicate phases but it is understood that real pastes, and in particular LAC formulations [22, 29], include significant amounts of aluminium. The influence of aluminium on low-pH pastes will thus have to be investigated.

Finally, to be complete, it must be emphasised that one of the main shortcomings of these model synthetic pastes was their tendency to crack; the density of cracks increased when the C/S ratio decreased. This was assumed to be an intrinsic property due to the polymerisation of the C-S-H induced by incorporation of silicate in the C-S-H during the pozzolanic reaction. Indeed, chain length variation is known to generate change in volume [27]. Yet the reader should keep in mind that the unusually high superplasticizer dosage might have also played a significant role in the brittleness of the model pastes. Shaping test samples for transport studies will thus require particular care.

Acknowledgments

The financial support for this work was provided by IRSN and CEA. Helpful discussions with Prof. B. Lothenbach (EMPA, Switzerland) and Prof. J. Skibsted (Aarhus University) are gratefully acknowledged.

References

[1] N. Seigneur, É. Kangni-Foli, V. Lagneau, A. Dauzères, S. Poyet, P. Le Bescop, E. L'Hôpital, J.B. d'Espinose de Lacaillerie, Understanding the effects of the atmospheric carbonation of cementitious materials using reactive transport modelling, Cem. Concr. Res. 130 (2020) 105966. doi:10.1016/j.cemconres.2019.105966.

[2] K. Ioannidou, K.J. Krakowiak, M. Bauchy, C.G. Hoover, E. Masoero, S. Yip, F.-J. Ulm, P. Levitz, R.J.-M. Pellenq, E. Del Gado, Mesoscale texture of cement hydrates, Proc. Natl. Acad. Sci. 113 (2016) 2029–2034. doi:10.1073/pnas.1520487113.

[3] J. Ollivier, J. Torrenti, La structure poreuse des bétons et les propriétés de transfert, La Durabilité Des Bétons. (2008) 51–133.

[4] K.L. Scrivener, A.K. Crumbie, P. Laugesen, The Interfacial Transition Zone (ITZ) Between Cement Paste and Aggregate in Concrete, Interface Sci. 12 (2004) 411–421. doi:10.1023/B:INTS.0000042339.92990.4c.

[5] J.S. Dolado, K. van Breugel, Recent advances in modeling for cementitious materials, Cem. Concr. Res. 41 (2011) 711–726. doi:10.1016/j.cemconres.2011.03.014.

[6] A. Dauzeres, P. Le Bescop, P. Sardini, C. Cau Dit Coumes, Physico-chemical investigation of clayey/cement-based materials interaction in the context of geological waste disposal: Experimental approach and results, Cem. Concr. Res. 40 (2010) 1327–1340. doi:10.1016/j.cemconres.2010.03.015.

[7] P. Lalan, A. Dauzères, L. De Windt, J. Sammaljärvi, D. Bartier, I. Techer, V. Detilleux, M. Siitari-Kauppi, Mineralogical and microstructural evolution of Portland cement paste/argillite interfaces at 70 °C – Considerations for diffusion and porosity properties, Cem. Concr. Res. 115 (2019) 414–425. doi:10.1016/j.cemconres.2018.09.018.

[8] C. Carde, R. François, J.-M. Torrenti, Leaching of both calcium hydroxide and C-S-H from cement paste: Modeling the mechanical behavior, Cem. Concr. Res. 26 (1996) 1257–1268. doi:10.1016/0008-8846(96)00095-6.

[9] C. Carde, R. François, Effect of the leaching of calcium hydroxide from cement paste on mechanical and physical properties, Cem. Concr. Res. 27 (1997) 539–550.

[10] E. Drouet, S. Poyet, P. Le Bescop, J.-M. Torrenti, X. Bourbon, Carbonation of hardened cement pastes: Influence of temperature, Cem. Concr. Res. (2019). doi:10.1016/J.CEMCONRES.2018.09.019.

[11] D. Planel, J. Sercombe, P. Le Bescop, F. Adenot, J.M. Torrenti, Long-term performance of cement paste during combined calcium leaching-sulfate attack: Kinetics and size effect, Cem. Concr. Res. 36 (2006) 137–143. doi:10.1016/j.cemconres.2004.07.039.

[12] X. Cong, R.J. Kirkpatrick, 29Si MAS NMR study of the structure of calcium silicate hydrate, Adv. Cem. Based Mater. 3 (1996) 144–156. doi:10.1016/S1065-7355(96)90046-2.

[13] A. Nonat, X. Lecoq, The Structure, Stoichiometry and Properties of C-S-H Prepared by C3S Hydration Under Controlled Condition, in: P. Colombet, A.-R. Grimmer, H. Zanni, P. Sozzani (Eds.), Nucl. Magn. Reson. Spectrosc. Cem. Mater., Springer, 1998: pp. 197–207. doi:10.1007/978-3-642-80432-8_14.

[14] I.F. Sáez Del Bosque, M. Martín-Pastor, I. Sobrados, S. Martínez-Ramírez, M.T. Blanco-Varela, Quantitative analysis of pure triclinic tricalcium silicate and C-S-H gels by29Si NMR longitudinal relaxation time, Constr. Build. Mater. 107 (2016) 52–57. doi:10.1016/j.conbuildmat.2015.12.146.

[15] K.O. Kjellsen, H. Justnes, Revisiting the microstructure of hydrated tricalcium silicate––a comparison to Portland cement, Cem. Concr. Compos. 26 (2004) 947–956. doi:10.1016/j.cemconcomp.2004.02.030.

[16] A. Helmuth, H. Turk, Elastic Moduli of Hardened Portland Cement and Tricalcium Silicate Pastes : Effect of Porosity, Portl. Cem. Assoc R D Lab Bull. 144 (1966) 135–144.

[17] J. Hagymassy, I. Odler, M. Yudenfreund, J. Skalny, S. Brunauer, Pore structure analysis by water vapor adsorption. III. Analysis of hydrated calcium silicates and portland cements, J. Colloid Interface Sci. 38 (1972) 20–34. doi:10.1016/0021-9797(72)90215-9.

[18] G. Geng, R. Taylor, S. Bae, D. Hernández-Cruz, D.A. Kilcoyne, A.-H. Emwas, P.J.M. Monteiro, Atomic and nano-scale characterization of a 50-year-old hydrated C3S paste, Cem. Concr. Res. 77 (2015) 36–46. doi:10.1016/j.cemconres.2015.06.010.

[19] E. Pustovgar, R.P. Sangodkar, A.S. Andreev, M. Palacios, B.F. Chmelka, R.J. Flatt, J.-B. d'Espinose de Lacaillerie, Understanding silicate hydration from quantitative analyses of hydrating tricalcium silicates, Nat. Commun. 7 (2016) 10952. doi:10.1038/ncomms10952.

[20] M. Codina, C. Cau-dit-Coumes, P. Le Bescop, J. Verdier, J.P. Ollivier, Design and characterization of low-heat and low-alkalinity cements, Cem. Concr. Res. 38 (2008) 437–448. doi:10.1016/j.cemconres.2007.12.002.

[21] H. Sakamoto, K. Haga, H. Fujita, K. Ishizaki, H. Amano, M. Hironaga, S. Nagasaki, S. Tanaka, pH Behavior of Hydrated Low-Alkalinity Cement, J. Nucl. Fuel Cycle Environ. 5 (1999) 37–42. doi:10.3327/jnuce.5.37.

[22] B. Lothenbach, G. Le Saout, M. Ben Haha, R. Figi, E. Wieland, Hydration of a low-alkali CEM III/B–SiO2 cement (LAC), Cem. Concr. Res. 42 (2012) 410–423. doi:10.1016/j.cemconres.2011.11.008.

[23] M. Auroy, S. Poyet, P. Le Bescop, J.M. Torrenti, T. Charpentier, M. Moskura, X. Bourbon, Impact of carbonation on unsaturated water transport properties of cement-based materials, Cem. Concr.

Res. 74 (2015) 44–58. doi:10.1016/j.cemconres.2015.04.002.

[24] K. Iriya, A. Matsui, M. Mihara, Study on applicability of HFSC for radioactive waste repositories, in: ASME (Ed.), Radioact. Waste Manag. Environ. Remediat. (ASME 1999), Nagoya (Japan), 1999. doi:10.1081/E-EEE2-120046011.

[25] C. Cau Dit Coumes, S. Courtois, D. Nectoux, S. Leclercq, X. Bourbon, Formulating a low-alkalinity, high-resistance and low-heat concrete for radioactive waste repositories, Cem. Concr. Res. 36 (2006) 2152–2163. doi:10.1016/j.cemconres.2006.10.005.

[26] J.J. Thomas, J.J. Chen, A.J. Allen, H.M. Jennings, Effects of decalcification on the microstructure and surface area of cement and tricalcium silicate pastes, Cem. Concr. Res. 34 (2004) 2297–2307. doi:10.1016/j.cemconres.2004.04.007.

[27] J.J. Chen, J.J. Thomas, H.M. Jennings, Decalcification shrinkage of cement paste, Cem. Concr. Res. 36 (2006) 801–809. doi:10.1016/j.cemconres.2005.11.003.

[28] J.J. Beaudoin, B. Patarachao, L. Raki, J. Margeson, R. Alizadeh, Length change of C–S–H of variable composition immersed in aqueous solutions, Adv. Cem. Res. 22 (2010) 15–20. doi:10.1680/adcr.2008.22.1.15.

[29] R.F. Feldman, Factors affecting young's modulus — Porosity relation of hydrated portland cement compacts, Cem. Concr. Res. 2 (1972) 375–386. doi:10.1016/0008-8846(72)90054-3.

[30] P.J. Sereda, R.F. Feldman, Compacts of powdered material as porous bodies for use in sorption studies, J. Appl. Chem. 13 (1963) 150–158. doi:10.1002/jctb.5010130402.

[31] Y. Wang, Q. Yuan, D. Deng, T. Ye, L. Fang, Measuring the pore structure of cement asphalt mortar by nuclear magnetic resonance, Constr. Build. Mater. 137 (2017) 450–458. doi:10.1016/j.conbuildmat.2017.01.109.

[32] W.A. Gutteridge, L.J. Parrott, A study of the changes in weight, length and interplanar spacing induced by drying and rewetting synthetic CSH (I), Cem. Concr. Res. 6 (1976) 357–366. doi:10.1016/0008-8846(76)90098-3.

[33] E.M. Foley, J.J. Kim, M.M.R. Taha, Synthesis and nano-mechanical characterization of calcium-silicate-hydrate (C-S-H) made with 1.5 CaO / SiO2 mixture, Cem. Concr. Res. 42 (2012) 1225–1232. doi:10.1016/j.cemconres.2012.05.014.

[34] P. Pourbeik, J.J. Beaudoin, R. Alizadeh, L. Raki, Correlation between dynamic mechanical thermo-analysis and composition-based models for C-S-H in hydrated portland cement paste, Mater. Struct. 48 (2015) 2447–2454. doi:10.1617/s11527-014-0330-7.

[35] R. Khoshnazar, J.J. Beaudoin, L. Raki, R. Alizadeh, Durability and mechanical properties of C–S–H/nitrobenzoic acid composite systems, Mater. Struct. 49 (2016) 5315–5325. doi:10.1617/s11527-016-0862-0.

[36] E. Bernard, B. Lothenbach, C. Cau-Dit-Coumes, C. Chlique, A. Dauzères, I. Pochard, Magnesium and calcium silicate hydrates, Part I: Investigation of the possible magnesium incorporation in calcium silicate hydrate (C-S-H) and of the calcium in magnesium silicate hydrate (M-S-H), Appl. Geochemistry. 89 (2018) 229–242. doi:10.1016/j.apgeochem.2017.12.005.

[37] E. Bernard, B. Lothenbach, F. Le Goff, I. Pochard, A. Dauzères, Effect of magnesium on calcium silicate hydrate (C-S-H), Cem. Concr. Res. 97 (2017) 61–72. doi:10.1016/j.cemconres.2017.03.012.

[38] H. Yang, Y. Che, F. Leng, Calcium leaching behavior of cementitious materials in hydrochloric acid solution, Sci. Rep. 8 (2018) 1–9. doi:10.1038/s41598-018-27255-x.

[39] Y.S. Choi, E.I. Yang, Effect of calcium leaching on the pore structure, strength, and chloride penetration resistance in concrete specimens, Nucl. Eng. Des. 259 (2013) 126–136. doi:10.1016/j.nucengdes.2013.02.049.

[40] P.J. Sereda, R.F. Feldman, E.G. Swenson, Effect of sorbed water on some mechanical properties of hydrated Portland cement pastes and compacts, Spec. Rep. Highw. Res. Board. 90 (1967) 58–73. doi:10.1039/J19710002393.

[41] W. Kunther, S. Ferreiro, J. Skibsted, Influence of the Ca/Si ratio on the compressive strength of cementitious calcium-silicate-hydrate binders, J. Mater. Chem. A. 5 (2017) 17401–17412. doi:10.1039/c7ta06104h.

[42] R. Maddalena, K. Li, P.A. Chater, S. Michalik, A. Hamilton, Direct synthesis of a solid calcium-silicate-hydrate (C-S-H), Constr. Build. Mater. 223 (2019) 554–565. doi:10.1016/j.conbuildmat.2019.06.024.

[43] L.G. Li, J.Y. Zheng, J. Zhu, A.K.H. Kwan, Combined usage of micro-silica and nano-silica in concrete: SP demand, cementing efficiencies and synergistic effect, Constr. Build. Mater. 168 (2018) 622–632. doi:10.1016/j.conbuildmat.2018.02.181.

[44] L. Nicoleau, A. Nonat, D. Perrey, The di- and tricalcium silicate dissolutions, Cem. Concr. Res. 47 (2013) 14–30. doi:10.1016/j.cemconres.2013.01.017.

[45] S. Garrault, Study of C-S-H growth on C3S surface during its early hydration, Mater. Struct. 38 (2005) 435–442. doi:10.1617/14343.

[46] H.F.W. Taylor, Cement chemistry, 2nd ed., Academic Press, London (UK), 1990. doi:10.1016/S0958-9465(98)00023-7.

[47] C. Rößler, F. Steiniger, H.-M. Ludwig, Characterization of C-S-H and C-A-S-H phases by electron microscopy imaging, diffraction, and energy dispersive X-ray spectroscopy, J. Am. Ceram. Soc. 100 (2017) 1733–1742. doi:10.1111/jace.14729.

[48] Z.-Q. Wu, J.F. Young, The hydration of tricalcium silicate in the presence of colloidal silica, J. Mater. Sci. 19 (1984) 3477–3486. doi:10.1007/BF02396922.

[49] K.O. Kjellsen, B. Lagerblad, Microstructure of tricalcium silicate and Portland cement systems at middle periods of hydration-development of Hadley grains, Cem. Concr. Res. 37 (2007) 13–20. doi:10.1016/j.cemconres.2006.09.008.

[50] M. Atkins, E.E. Lachowski, F.P. Glasser, Investigation of solid and aqueous chemistry of 10-year-old Portland cements pastes; with and without silica modifier, Adv. Cem. Res. 5 (1993) 97–102.

[51] K. Baltakys, R. Jauberthie, R. Jauberthie, R. Siauciunas, R. Kaminskas, Influence of modification of SiO2 on the formation of calcium silicate hydrate, Mater. Sci. 25 (2007) 663–670.

[52] R. Maddalena, C. Hall, A. Hamilton, Effect of silica particle size on the formation of calcium silicate hydrate [C-S-H] using thermal analysis, Thermochim. Acta. 672 (2019) 142–149. doi:10.1016/j.tca.2018.09.003.

[53] Z. Rong, W. Sun, H. Xiao, G. Jiang, Effects of nano-SiO2 particles on the mechanical and microstructural properties of ultra-high performance cementitious composites, Cem. Concr. Compos. 56 (2015) 25–31. doi:10.1016/j.cemconcomp.2014.11.001.

[54] G. Quercia, G. Hüsken, H.J.H. Brouwers, Water demand of amorphous nano silica and its impact on the workability of cement paste, Cem. Concr. Res. 42 (2012) 344–357. doi:10.1016/j.cemconres.2011.10.008.

[55] S. Abd.El.Aleem, M. Heikal, W.M. Morsi, Hydration characteristic, thermal expansion and microstructure of cement containing nano-silica, Constr. Build. Mater. 59 (2014) 151–160. doi:10.1016/j.conbuildmat.2014.02.039.

[56] R.K. Iler, Coagulation of colloidal silica by calcium ions, mechanism, and effect of particle size, J. Colloid Interface Sci. 53 (1975) 476–488. doi:10.1016/0021-9797(75)90065-X.

[57] E.A. Gorrepati, P. Wongthahan, S. Raha, H.S. Fogler, Silica precipitation in acidic solutions: Mechanism, pH effect, and salt effect, Langmuir. 26 (2010) 10467–10474. doi:10.1021/la904685x.

[58] V. Dutzer, W. Dridi, S. Poyet, P. Le Bescop, X. Bourbon, The link between gas diffusion and carbonation in hardened cement pastes, Cem. Concr. Res. 123 (2019) 105795. doi:10.1016/j.cemconres.2019.105795.

[59] T.L.P. Hang, J. Verdier, T. Vidal, G. Camps, X. Bourbon, Mechanical and transfer properties of low-pH

concretes in view of classical HPC substitution in confinement structures, Eur. J. Environ. Civ. Eng. 23 (2019) 657–674. doi:10.1080/19648189.2017.1304274.

[60] M.C. Alonso, J.L. García Calvo, S. Petterson, I. Puigdomenech, M.A. Cunado, M. Vuorio, H. Weber, H. Ueda, M. Naito, C. Walker, Y. Takeshi, C. Cau Dit Coumes, Round Robin test for define an accurate protocol to measure the pore fluid pHof low-pH cementitious materials, in: SFEN (Ed.), Proc. 2nd Int. Symp. Cem. Mater. Nucl. Wastes, SFEN, Avignon, France, 2014: pp. 1–10.

[61] A. Behnood, K. van Tittelboom, N. de Belie, Methods for measuring pH in concrete : A review, Constr. Build. Mater. 105 (2016) 176–188. doi:10.1016/j.conbuildmat.2015.12.032.

[62] G. Plusquellec, M.R. Geiker, J. Lindgård, J. Duchesne, B. Fournier, K. De Weerdt, Determination of the pH and the free alkali metal content in the pore solution of concrete: Review and experimental comparison, Cem. Concr. Res. 96 (2017) 13–26. doi:10.1016/j.cemconres.2017.03.002.

[63] G. Villain, M. Thiery, G. Platret, Measurement methods of carbonation profiles in concrete: thermogravimetry, chemical analysis and gammadensimetry, Cem. Concr. Res. 37 (2007) 1182–1192. doi:10.1016/j.cemconres.2007.04.015.

[64] B. Lothenbach, P. Durdzinski, K. De Weerdt, Thermogravimetric analysis, in: K. Scrivener, R. Snellings, B. Lothenbach (Eds.), A Pract. Guid. to Microstruct. Anal. Cem. Mater., CRC Press, Boca Raton (USA), 2016: pp. 177–211.

[65] F. Angeli, M. Gaillard, P. Jollivet, T. Charpentier, Contribution of 43Ca MAS NMR for probing the structural configuration of calcium in glass, Chem. Phys. Lett. 440 (2007) 324–328. doi:10.1016/j.cplett.2007.04.036.

[66] T. Charpentier, Résonance magnétique nucléaire haute-résolution des noyaux quadrupolaires dans les solides. PhD thesis, (in French), 1998.

[67] AFNOR, Essai pour béton durci : essai de porosité et de masse volumique (in French), Stand. NF P18-459. (2010) 9p.

[68] R.A. Olson, H.M. Jennings, Estimation of C-S-H content in a blended cement paste using water adsorption, Cem. Concr. Res. 31 (2001) 351–356. doi:10.1016/S0008-8846(01)00454-9.

[69] S. Poyet, K. Trentin, E. Amblard, The Use of Sorption Balance for the Characterization of the Water Retention Curve of Cement-Based Materials, J. Adv. Concr. Technol. 14 (2016) 354–367. doi:10.3151/jact.14.354.

[70] G.W. Groves, A. Brough, I.G. Richardson, C.M. Dobson, Progressive changes in the structure of hardened C3S cement pastes due to carbonation, J. Am. Ceram. Soc. 74 (1991) 2891–2896.

[71] I.G. Richardson, G.W. Groves, Models for the composition and structure of calcium silicate hydrate (CSH) gel in hardened tricalcium silicate pastes, Cem. Concr. Res. 22 (1992) 1001–1010. doi:10.1016/0008-8846(92)90030-Y.

[72] J.W. Bullard, J. Hagedorn, T.M. Ley, Q. Hu, W. Griffin, J.E. Terrill, A critical comparison of 3D experiments and simulations of tricalcium silicate hydration, J. Am. Ceram. Soc. 101 (2018) 1453–1470. doi:10.1111/jace.15323.

[73] Z. Xu, Z. Zhou, P. Du, X. Cheng, Effects of nano-silica on hydration properties of tricalcium silicate, Constr. Build. Mater. J. 125 (2016) 1169–1177. doi:10.1016/j.conbuildmat.2016.09.003.

[74] S. Grangeon, F. Claret, Y. Linard, C. Chiaberge, X-ray diffraction: A powerful tool to probe and understand the structure of nanocrystalline calcium silicate hydrates, Acta Crystallogr. Sect. B Struct. Sci. Cryst. Eng. Mater. 69 (2013) 465–473. doi:10.1107/S2052519213021155.

[75] S. Merlino, E. Bonaccorsi, T. Armbruster, The real structure of tobermorite 11A: normal and anomalous forms, OD character and polytypic modifications, Eur. J. Mineral. 13 (2001) 577–590. doi:10.1127/0935-1221/2001/0013-0577.

[76] E. Bonaccorsi, S. Merlino, H.F.W. Taylor, The crystal structure of jennite, Ca9Si6O18(OH)6·8H2O, Cem. Concr. Res. 34 (2004) 1481–1488. doi:10.1016/j.cemconres.2003.12.033.

[77] A. Dauzères, Etude expérimentale et modélisation des mécanismes physico-chimiques des interactions béton-argile dans le contexte du stockage géologique des déchets radioactifs (in french), Ph.D. Thesis, University Poitiers (France), 2010.

[78] M. Auroy, Impact de la carbonatation sur les propriétés de transport d'eau des matériaux cimentaires (in french), Ph.D. Thesis, Université Paris-Est (France), 2014.

[79] E. Drouet, S. Poyet, J.-M. Torrenti, Temperature influence on water transport in hardened cement pastes, Cem. Concr. Res. 76 (2015) 37–50. doi:10.1016/j.cemconres.2015.05.002.

[80] I. Klur, B. Pollet, J. Virlet, A. Nonat, C-S-H Structure Evolution with Calcium Content by Multinuclear NMR, in: Nucl. Magn. Reson. Spectrosc. Cem. Mater., Springer Berlin Heidelberg, Berlin, Heidelberg, 1998: pp. 119–141. doi:10.1007/978-3-642-80432-8_8.

[81] M.D. Andersen, H.J. Jakobsen, J. Skibsted, Characterization of white Portland cement hydration and the C-S-H structure in the presence of sodium aluminate by 27Al and 29Si MAS NMR spectroscopy, Cem. Concr. Res. 34 (2004) 857–868. doi:10.1016/j.cemconres.2003.10.009.

[82] I. Klur, J.-F. Jacquinot, F. Brunet, T. Charpentier, J. Virlet, C. Schneider, P. Tekely, NMR Cross-Polarization when T IS > T 1 ρ ; Examples from Silica Gel and Calcium Silicate Hydrates, J. Phys. Chem. B. 104 (2000) 10162–10167. doi:10.1021/jp001342u.

[83] T.F. Sevelsted, J. Skibsted, Carbonation of C-S-H and C-A-S-H samples studied by 13C, 27Al and 29Si MAS NMR spectroscopy, Cem. Concr. Res. 71 (2015) 56–65. doi:10.1016/j.cemconres.2015.01.019.

[84] S. Grangeon, F. Claret, C. Roosz, T. Sato, S. Gaboreau, Y. Linard, Structure of nanocrystalline calcium silicate hydrates: Insights from X-ray diffraction, synchrotron X-ray absorption and nuclear magnetic resonance, J. Appl. Crystallogr. 49 (2016) 771–783. doi:10.1107/S1600576716003885.

[85] I.G. Richardson, G.W. Groves, Microstructure and microanalysis of hardened ordinary Portland cement pastes, J. Mater. Sci. 28 (1993) 265–277. doi:10.1007/BF00349061.

[86] J.E. Rossen, B. Lothenbach, K.L. Scrivener, Composition of C-S-H in pastes with increasing levels of silica fume addition, Cem. Concr. Res. 75 (2015) 14–22. doi:10.1016/j.cemconres.2015.04.016.

[87] J. Haas, A. Nonat, From C-S-H to C-A-S-H: Experimental study and thermodynamic modelling, Cem. Concr. Res. 68 (2015) 124–138. doi:10.1016/j.cemconres.2014.10.020.

[88] E.P. Flint, L.S. Wells, Study of the system CaO-SiO2-H2O at 30 C and of the reaction of water on the anhydrous calcium silicates, Bur. Stand. J. Res. 12 (1934) 33. doi:10.6028/jres.012.060.

[89] M. Grutzeck, A. Benesi, B. Fanning, Silicon-29 Magic Angle Spinning Nuclear Magnetic Resonance Study of Calcium Silicate Hydrates, J. Am. Ceram. Soc. 72 (1989) 665–668. http://onlinelibrary.wiley.com/doi/10.1111/j.1151-2916.1989.tb06192.x/abstract.

[90] J.J. Chen, J.J. Thomas, H.F.W. Taylor, H.M. Jennings, Solubility and structure of calcium silicate hydrate, Cem. Concr. Res. 34 (2004) 1499–1519. doi:10.1016/j.cemconres.2004.04.034.

[91] S.A. Greenberg, T.N. Chang, Investigation of the Colloidal Hydrated Calcium Silicates. II. Solubility Relationships in the Calcium Oxide-Silica-Water System at 25°, J. Phys. Chem. 69 (1965) 182–188. doi:10.1021/j100885a027.

[92] K. Suzuki, T. Nishikawa, S. Ito, Formation and carbonation of C-S-H in water, Cem. Concr. Res. 15 (1985) 213–224. doi:10.1016/0008-8846(85)90032-8.

[93] A. Atkinson, J.A. Hearne, C.F. Knights, Aqueous chemistry and thermodynamic modelling of CaO–SiO2 –H2O gels, J. Chem. Soc., Dalt. Trans. 0 (1989) 2371–2379. doi:10.1039/DT9890002371.

[94] M. Atkins, F.P. Glasser, A. Kindness, Cement hydrate phase: Solubility at 25°C, Cem. Concr. Res. 22 (1992) 241–246. doi:10.1016/0008-8846(92)90062-Z.

[95] A.. Harris, M.. Manning, W.. Tearle, C.. Tweed, Testing of models of the dissolution of cements—leaching of synthetic CSH gels, Cem. Concr. Res. 32 (2002) 731–746. doi:10.1016/S0008-8846(01)00748-7.

[96] J. Hill, A.W. Harris, M. Manning, A. Chambers, S.W. Swanton, The effect of sodium chloride on the dissolution of calcium silicate hydrate gels, Waste Manag. 26 (2006) 758–768. doi:https://doi.org/10.1016/j.wasman.2006.01.022.

[97] C.S. Walker, D. Savage, M. Tyrer, K.V. Ragnarsdottir, Non-ideal solid solution aqueous solution modeling of synthetic calcium silicate hydrate, Cem. Concr. Res. 37 (2007) 502–511. doi:10.1016/j.cemconres.2006.12.002.

[98] D. Sugiyama, Chemical alteration of calcium silicate hydrate (C–S–H) in sodium chloride solution, Cem. Concr. Res. 38 (2008) 1270–1275. doi:10.1016/j.cemconres.2008.06.002.

[99] V.S. Ramachandran, Interaction of calcium lignosulfonate with tricalcium silicate, hydrated tricalcium silicate and calcium hydroxide, Cem. Concr. Resear. 2 (1972) 179–194.

[100] R. Flatt, I. Schober, Superplasticizers and the rheology of concrete, in: N. Roussel (Ed.), Underst. Rheol. Concr., Woodhead Publishing Limited, 2012: pp. 144–208. doi:10.1533/9780857095282.2.144.

[101] A. Popova, G. Geoffroy, M.-F. Renou-Gonnord, P. Faucon, E. Gartner, Interactions between Polymeric Dispersants and Calcium Silicate Hydrates, J. Am. Ceram. Soc. 83 (2000) 2556–2560. doi:10.1111/j.1151-2916.2000.tb01590.x.

[102] A. Popova, G. Geoffroy, E.M. Gartner, A. Lapp, Calcium Silicate Hydrates studied by Small-Angle Neutron Scattering (SANS), J. Am. Ceram. Soc. 85 (2002) 1303–1305.

[103] J. Sun, H. Shi, B. Qian, Z. Xu, W. Li, X. Shen, Effects of synthetic C-S-H/PCE nanocomposites on early cement hydration, Constr. Build. Mater. 140 (2017) 282–292. doi:10.1016/j.conbuildmat.2017.02.075.

[104] V. Kanchanason, J. Plank, Role of pH on the structure, composition and morphology of C-S-H–PCE nanocomposites and their effect on early strength development of Portland cement, Cem. Concr. Res. 102 (2017) 90–98. doi:10.1016/j.cemconres.2017.09.002.

[105] J. Plank, M. Schönlein, V. Kanchanason, Study on the early crystallization of calcium silicate hydrate (C-S-H) in the presence of polycarboxylate superplasticizers, J. Organomet. Chem. 869 (2018) 227–232. doi:10.1016/j.jorganchem.2018.02.005.

[106] V. Kanchanason, J. Plank, Effectiveness of a calcium silicate hydrate – Polycarboxylate ether (C-S-H–PCE) nanocomposite on early strength development of fly ash cement, Constr. Build. Mater. 169 (2018) 20–27. doi:10.1016/j.conbuildmat.2018.01.053.

[107] I.G. Richardson, Model structures for C-(A)-S-H(I), Acta Crystallogr. Sect. B Struct. Sci. Cryst. Eng. Mater. 70 (2014) 903–923. doi:10.1107/S2052520614021982.

[108] A. Nonat, The structure and stoichiometry of C-S-H, Cem. Concr. Res. 34 (2004) 1521–1528. doi:10.1016/j.cemconres.2004.04.035.

[109] I. García-Lodeiro, A. Fernández-Jiménez, I. Sobrados, J. Sanz, A. Palomo, C-S-H gels: Interpretation of 29Si MAS-NMR spectra, J. Am. Ceram. Soc. 95 (2012) 1440–1446. doi:10.1111/j.1551-2916.2012.05091.x.

[110] Y. He, L. Lu, L.J. Struble, J.L. Rapp, P. Mondal, S. Hu, Effect of calcium–silicon ratio on microstructure and nanostructure of calcium silicate hydrate synthesized by reaction of fumed silica and calcium oxide at room temperature, Mater. Struct. 47 (2013) 311–322. doi:10.1617/s11527-013-0062-0.

[111] E. L'Hôpital, B. Lothenbach, D.A. Kulik, K. Scrivener, Influence of calcium to silica ratio on aluminium uptake in calcium silicate hydrate, Cem. Concr. Res. 85 (2016) 111–121. doi:10.1016/j.cemconres.2016.01.014.

[112] R.J. Myers, S.A. Bernal, R. San Nicolas, J.L. Provis, Generalized structural description of calcium-sodium aluminosilicate hydrate gels: The cross-linked substituted tobermorite model, Langmuir. 29 (2013) 5294–5306. doi:10.1021/la4000473.

Supplementary materials

Appendix A: details of the batching sequence.

The final batching sequence obtained for the model pastes including nanosilica was as follows:

1. Addition of C_3S in the planetary mixer (mixing speed at 95 rpm).
2. Addition of all the water, including half of the total amount of SP.
3. Mixing at 250 rpm for 30 s.
4. Slow incorporation of nanosilica (at 400 rpm) while monitoring the fresh mix rheology to avoid flocculation and a viscosity increase that could eventually make it irreversibly unworkable. Addition of SP to maintain the workability of the fresh mix. The duration of this step depended on the amount of nanosilica added (Table 1).
5. Preparation of the test specimens: the paste was poured into polytetrafluoroethylene (PTFE) moulds (Ø30 × H110 mm) and vibrated. This phase proved complicated due to the strong thixotropic behaviour of the fresh mix, which worsened when the silica content was increased.
6. The specimens were kept one month in their sealed moulds at ambient temperature. After unmoulding, they were cured for two more months under a batch of water to which small amounts of crushed samples were added to ensure that chemical equilibrium was reached in the curing solution.
7. Finally, the samples were left to dry in a glovebox at 20°C and 55% RH. It is presumed that under these conditions, hydration did not proceed significantly anymore.

Appendix B: decomposition of NMR spectra.

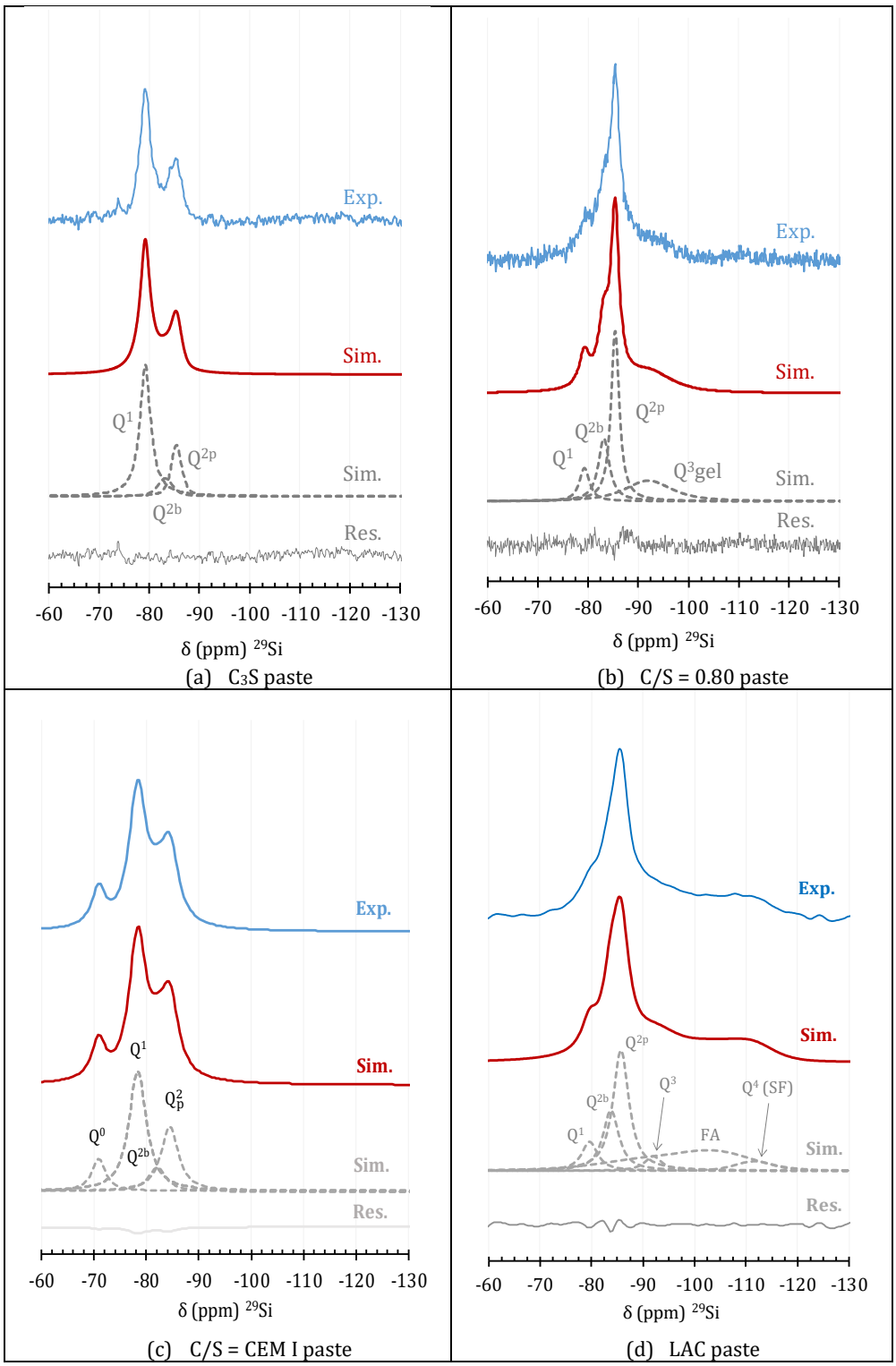

Figure S 1: Examples of decomposition of ^{29}Si NMR spectra.

Table S 1: Parameters of the decomposition of the ^{29}Si NMR spectra of the synthetic pastes. No Q^0 peak was considered for the C_3S paste as its contribution was of the order of the noise.

C/S ratio		0.8-3.00
Q^1	δ (ppm)	-79.2
	FWHM (ppm)	2.9
	Ratio L/G	1.0
	GB	1.02
Q^2_b	δ (ppm)	-83.1
	FWHM (ppm)	2.9
	Ratio L/G	0.5
	GB	1.1
Q^2_p	δ (ppm)	-85.4
	FWHM (ppm)	2.21
	Ratio L/G	1.0
	GB	0.5
Q^3 + Q^3gel	δ (ppm)	-92
	FWHM (ppm)	11.3
	Ratio L/G	0.5
	GB (ppm)	4.7
G = Gaussian lineshape L = Lorentzian lineshape GB = Gaussian enhancement		

784

Appendix C: diffractogram of the reference system

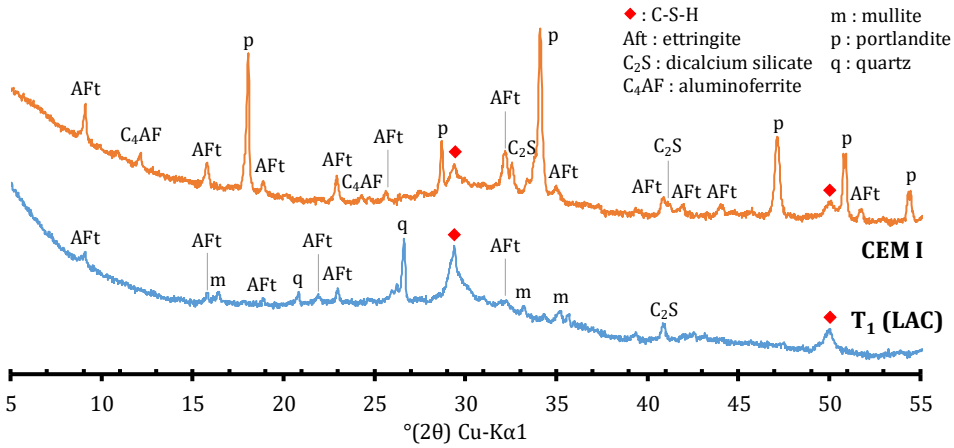

Figure S 2: Diffractograms of the two reference pastes. For the OPC (CEM I) paste, besides aluminates, C-S-H and portlandite signals were observed. No portlandite reflections were present in the LAC (CEM I + SF + FA) paste. Besides the C-S-H signal, an intense diffuse background located between 20-28 °(2θ) typical of unreacted silica and small reflections of quartz occurred. ICDD CH: 44-1481; AFt:41-1451; mullite: 15-0776; C_4AF: 30-0226; C_2S: 31-0302.

Appendix D: Chemical composition of the components of the synthetic model and reference pastes

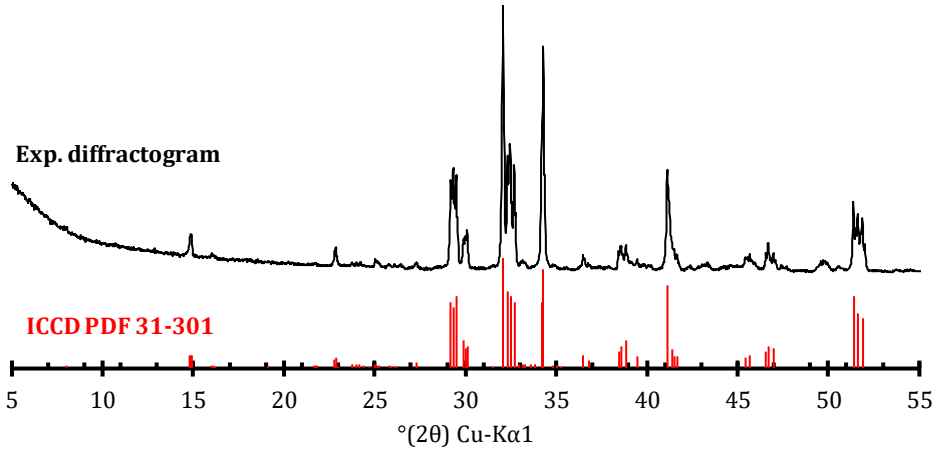

Figure S 3: diffractogram of the C_3S used for the preparation of the synthetic model pastes

Main properties of the colloidal silica suspension (Rheomac AS 150):

- density = 1.40 ± 0.02 g.cm^{-3};
- pH = 10 ± 1.5;
- Cl < 0.1 wt%;
- Na_2O_{eq} < 1.0 wt%

Table S 2: chemical composition of the LAC reference pastes' components, reproduced from [20]

Compounds	wt% of the compounds			wt% of the blend (LAC)
	CEM I 52.5	Silica fume	Fly Ash	
	Lafarge Le Teil	Condensil S95 DM	EDF Cordemais	
CaO	67.41	0.40	5.52	27.0
SiO_2	22.84	95.00	49.48	54.3
Al_2O_3	2.70	0.60	29.17	10.0
Fe_2O_3	1.84	<0.05	6.23	2.6
MgO	0.81	0.30	2.08	1.0
MnO	-	-	0.08	-
Na_2O	0.14	<0.20	0.58	0.3
K_2O	0.23	0.29	1.22	0.5
SO_3	2.23	<0.20	0.64	1.1
S^{2-}	<0.01	<0.10	-	
P_2O_5	-	-	0.70	
TiO_2	-	-	1.61	
LOI	1.72	3.10	2.20	
LOI = loss on ignition (1000 °C)				

Table S 3: chemical composition of the OPC used for the preparation of the OPC reference paste

Compounds	CEM I 52.5
	Lafarge Val d'Azergues
CaO	65.0
SiO_2	21.0
Al_2O_3	3.4
Fe_2O_3	4.5
MgO	0.62
MnO	-
Na_2O	0.09
K_2O	0.72
SO_3	2.71
S^{2-}	<0.01
P_2O_5	0.50
TiO_2	-
LOI	1.30
LOI = Loss on ignition (1000 °C)	

811